Research Article

EASL JOURNAL OF HEPATOLOGY

Impact of higher-order heme degradation products on hepatic function and hemodynamics

Graphical abstract

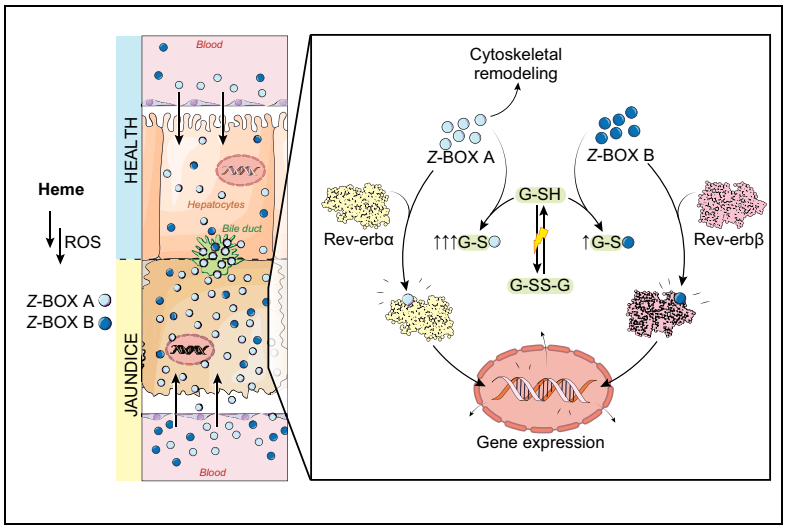

Highlights

- Plasma levels of bilirubin oxidation products rise in cholestatic liver disease.
- The regio-isomers *Z*-BOX A and B exhibit distinct pharmacokinetics and -dynamics.
- *Z*-BOX A and B differentially affect the hepatocellular glutathione redox state.
- *Z*-BOX A and B differentially modulate the activity of Rev-erbα and Rev-erbβ.

Authors

Raphael A. Seidel, Thierry Claudel, Franziska A. Schleser, ..., Georg Pohnert, Michael Trauner, Michael Bauer

Correspondence

michael.bauer@med.uni-jena.de (Michael Bauer)

Lay summary

Degradation of the blood pigment heme yields the bile pigment bilirubin and the oxidation products *Z*-BOX A and *Z*-BOX B. Serum concentrations of these bioactive molecules increase in jaundice and can impair liver function and integrity. Amounts of *Z*-BOX A and *Z*-BOX B that are observed during liver failure in humans have profound effects on hepatic function when added to cultured liver cells or infused into healthy rats.

http://dx.doi.org/10.1016/j.jhep.2017.03.037
European Association for the Study of the Liver J. Hepatol. 2017, 67, 272–281

Research Article

JOURNAL OF HEPATOLOGY

Impact of higher-order heme degradation products on hepatic function and hemodynamics

Raphael A. Seidel[1,2], Thierry Claudel[3], Franziska A. Schleser[1], Navin K. Ojha[4], Matthias Westerhausen[5], Sandor Nietzsche[6], Christoph Sponholz[1], Frans Cuperus[3,7], Sina M. Coldewey[1], Stefan H. Heinemann[4], Georg Pohnert[2], Michael Trauner[3,†], Michael Bauer[1,*,†]

[1]*Department of Anesthesiology and Intensive Care Medicine/Center for Sepsis Control and Care, Jena University Hospital, Germany;* [2]*Institute of Inorganic and Analytical Chemistry, Bioorganic Analytics, Friedrich Schiller University Jena, Germany;* [3]*HansPopper Laboratory of Molecular Hepatology, Division of Gastroenterology and Hepatology, Department of Internal Medicine III, Medical University of Vienna, Austria;* [4]*Center for Molecular Biomedicine, Department of Biophysics, Friedrich Schiller University Jena & Jena University Hospital, Germany;* [5]*Institute of Inorganic and Analytical Chemistry, Inorganic Chemistry I, Friedrich Schiller University Jena, Germany;* [6]*Electron Microscopy Center, Jena University Hospital, Germany;* [7]*Pediatric Gastroenterology and Hepatology, Center for Liver, Digestive, and Metabolic Diseases, University Medical Center Groningen, The Netherlands*

See Editorial, pages 214–215

Background & Aims: Biliverdin and bilirubin were previously considered end products of heme catabolism; now, however, there is evidence for further degradation to diverse bioactive products. *Z*-BOX A and *Z*-BOX B arise upon oxidation with unknown implications for hepatocellular function and integrity. We studied the impact of *Z*-BOX A and B on hepatic functions and explored their alterations in health and cholestatic conditions.
Methods: Functional implications and mechanisms were investigated in rats, hepatocytic HepG2 and HepaRG cells, human immortalized hepatocytes, and isolated perfused livers. *Z*-BOX A and B were determined by liquid chromatography-tandem mass spectrometry (LC-MS/MS) in acute and acute-on-chronic liver failure and hereditary unconjugated hyperbilirubinemia.
Results: *Z*-BOX A and B are found in similar amounts in humans and rodents under physiological conditions. Serum concentrations increased ~20-fold during cholestatic liver failure in humans ($p < 0.001$) and in hereditary deficiency of bilirubin glucuronidation in rats ($p < 0.001$). Pharmacokinetic studies revealed shorter serum half-life of *Z*-BOX A compared to its regio-isomer *Z*-BOX B ($p = 0.035$). While both compounds were taken up by hepatocytes, *Z*-BOX A was enriched ~100-fold and excreted in bile. Despite their reported vasoconstrictive properties in the brain vasculature, BOXes did not affect portal hemodynamics. Both *Z*-BOX A and B showed dose-dependent cytotoxicity, affected the glutathione redox state, and differentially modulated activity of Rev-erbα and Rev-erbβ. Moreover, BOXes-triggered remodeling of the hepatocellular cytoskeleton.
Conclusions: Our data provide evidence that higher-order heme degradation products, namely *Z*-BOX A and B, impair hepatocellular integrity and might mediate intra- and extrahepatic cytotoxic effects previously attributed to hyperbilirubinemia.
Lay summary: Degradation of the blood pigment heme yields the bile pigment bilirubin and the oxidation products *Z*-BOX A and *Z*-BOX B. Serum concentrations of these bioactive molecules increase in jaundice and can impair liver function and integrity. Amounts of *Z*-BOX A and *Z*-BOX B that are observed during liver failure in humans have profound effects on hepatic function when added to cultured liver cells or infused into healthy rats.

Introduction

Heme (iron protoporphyrin IX) serves as a prosthetic group in a variety of proteins involved in oxygen transport, redox reactions, and signaling.[1] When released extracellularly, labile heme acts as an alarmin[2] and cytotoxic agonist[3] that is encountered by scavenger systems.[4] Intracellular heme concentrations are tightly controlled by its enzymatic degradation via heme oxygenases (HO),[5] yielding the first-order degradation products biliverdin, ferrous iron, and carbon monoxide (CO).[6,7] The induction of HO-1 reflects a hallmark of the cellular response to oxidative stress and confers tissue protection during infection and inflammation.[8,9] Bilirubin, generated from biliverdin by biliverdin reductases, contributes to tissue integrity via its anti-oxidative properties.[10,11] Nevertheless, above a certain threshold bilirubin is held responsible for intra- and extrahepatic dysfunction,

Keywords: Heme degradation; Bilirubin oxidation end products (BOXes); Bilirubin toxicity; Rev-erb; Glutathione; Cholestasis; Hemodynamics; Pharmacokinetics; Cytoskeleton; Reactive oxygen species.
Received 5 July 2016; received in revised form 13 March 2017; accepted 20 March 2017; available online 12 April 2017
* Corresponding author. Address: Department of Anesthesiology and Intensive Care Medicine, Jena University Hospital, Am Klinikum 1, 07747 Jena, Germany; Tel.: +49 3641 9 323101; fax: +49 3641 9 323102.
E-mail address: michael.bauer@med.uni-jena.de (M. Bauer).
† These authors share senior authorship.

including neurotoxicity and cholemic nephropathy.[12,13] In conditions of oxidative stress, unconjugated bilirubin is oxidized to higher-order degradation products such as the major bilirubin oxidation end products (BOXes), in particular the regio-isomers *Z*-2-(4-methyl-5-oxo-3-vinyl-1,5-dihydro-2H-pyrrol-2-ylidene)-acetamide (*Z*-BOX A) and *Z*-2-(3-methyl-5-oxo-4-vinyl-1,5-dihydro-2H-pyrrol-2-ylidene)acetamide (*Z*-BOX B)[14] (Fig. S1).

In subarachnoid hemorrhage, *Z*-BOX A and B mediate vasoconstriction, presumably via inhibition of large-conductance Ca^{2+}- and voltage-dependent Slo1 potassium channels.[15,16] However, systematic assessment of the role of these higher-order degradation products was hampered so far by a lack of analytical tools and BOXes of appropriate purity.[16–18] To enable the systematic assessment of biological fate and function, we recently established syntheses,[19,20] purification, and sensitive analytics of *Z*-BOX A and B.[21] Given the central role of the liver in heme degradation, we studied pharmacokinetics and -dynamics of *Z*-BOX A and B and explored their impact on hepatic function.

Materials and methods

Preparation of BOXes

Z-BOX A and *Z*-BOX B were prepared via *in vitro* bilirubin oxidation and chemical synthesis as described.[19,20] Isomer purity was confirmed by liquid chromatography, coupled to tandem mass spectrometry (LC-MS/MS) and nuclear magnetic resonance spectroscopy. Water solubility and partition constants (1-octanol/water) were determined spectrophotometrically.

Quantification of BOXes

Simultaneous determination of *Z*-BOX A and B was achieved via LC-MS/MS.[21] To assess possible differences between *Z*-BOXes concentrations in serum and plasma preparations human serum and plasma samples were spiked with 80 or 300 nmol·L^{-1} of both analytes and analyzed accordingly. Gallstones were extracted using acetonitrile/isopropanol/water (2/1/1, v/v/v; 10 µl·mg^{-1} concrement).

Human specimen collection

All biomaterials were collected after approval by the ethics committee of Jena University and with informed consent from all subjects or their legal representatives (3548-08/12; 2435-12/08; 3624-11/12; 2712-12/09; 2160-11/07; 4406-04/15). Plasma samples of 28 patients were obtained upon fulfilling diagnostic criteria for liver failure (acute, ALF, n = 9; acute-on-chronic, ACLF, n = 15; transplant failure, n = 4). Ten healthy volunteers served as controls.

Rodents

Male Wistar rats (286–539 g, Harlan Laboratories), homozygous Gunn rats (165–333 g, in-house breeding[22]), and C57BL/6J mice (25–30 g, in-house breeding) were used with the approval of the institutional animal welfare committees (Thuringian State Office for Consumer Protection and Food Safety, Bad Langensalza, Germany, 02-001/11, 02-058/14; Animal Ethics Committee of the University of Groningen, Groningen, The Netherlands, DEC6660A) under isoflurane anesthesia.

PK/PD studies

Rats were catheterized via the right jugular vein to inject *Z*-BOX A and *Z*-BOX B (26.7 µg·(kg body weight)$^{-1}$ in PBS containing 0.25% dimethyl sulfoxide, DMSO), the left carotid artery for blood sampling, and bile duct for bile collection. Urine was sampled before and 60 min after application.

Portal hemodynamics

Rat livers were perfused via the portal vein with carbogen-saturated Krebs Henseleit buffer (Biochrom, Berlin, Germany) containing 2 g·L^{-1} glucose, using a body weight-adapted constant flow rate of 100 ml·(kg body weight·min)$^{-1}$. *Z*-BOX A, *Z*-BOX B, or vehicle was individually administered to the main flow. In parallel to bile sampling, portal pressure was measured (TSD104A, 10 or 20 Hz, Biopac Systems, Goleta, CA, USA) and 0.01 Hz low-pass filtered (OriginLab, Northampton, USA).

Cell culture

All reagents were obtained from Life Technologies (Darmstadt, Germany), unless otherwise stated. HepG2 cells (DSMZ, Braunschweig, Germany; authenticated by short tandem repeats (STR) profiling) were cultured in the dark at 37°C using Dulbecco's Modified Eagle's Medium (DMEM)/Nutrient Mixture F-12 (1:1), supplemented with 10% fetal bovine serum (FBS), 1 µg·ml^{-1} streptomycin, and 1 U·ml^{-1} penicillin. Measurements of metabolic rate (MTT assay) and lactate dehydrogenase (LDH) release (Roche Diagnostics, Mannheim, Germany) were conducted according to the manufacturer's instructions, in medium containing 1% FBS after 96 h treatment with *Z*-BOX A, *Z*-BOX B, or vehicle control. EC_{50} values were calculated using the model $f = \min + (\max - \min)/(1 + 10^{\log EC50 - x})$. Changes in the intracellular glutathione redox potential were measured with a genetically encoded fluorescent sensor, consisting of a fusion of redox-sensitive green fluorescent protein (roGFP2) and glutaredoxin 1 (Grx1).[23] Ratiometric fluorescence measurements (400/470 nm; photodiode and Polychrome V monochromator, TILL Photonics, Munich, Germany) of individual HepG2 cells were performed after 1 h incubation with BOXes in culturing medium. HepaRG (INSERM Transfert, Paris, France) cells were cultured using Williams' E medium supplemented with 10% FBS, 2 mmol · L^{-1} glutamine, 2.5 ng · ml^{-1} insulin, 24.7 µg · ml^{-1} hydrocortisone 21-hemisuccinate, 1 µg · ml^{-1} streptomycin, and 1 U · ml^{-1} penicillin. Terminal differentiation was induced by supplementing 2% DMSO for two weeks. Morphology of HepG2 and HepaRG cells was studied after incubation with supraphysiological concentrations (500 µmol·L^{-1} or 700 µmol·L^{-1}) of *Z*-BOXes after 24 h and 48 h. Media containing *Z*-BOX A, *Z*-BOX B, and vehicle were prepared with 0.25% (HepG2) or 1.0% (HepaRG) DMSO. Human immortalized hepatocytes (HIH) were already described,[24] a subclone was obtained after serial passages and grown in DMEM with 10% FBS and 0.5% penicillin/streptomycin (ThermoFisher, Austria) and incubated for 48 h, with or without *Z*-BOX A or *Z*-BOX B at 15 µmol·L^{-1} or SR8278 (Tocris, Biomedica, Austria).

Quantitative real-time PCR (qPCR)

After RNA extraction (Trireagent) and retro-transcription (MMLV, Sigma, Austria), qPCR was performed using the SYBRgreen method (SYBR Select Master Mix; ABIprism 7500, ThermoFisher, Austria). Primer sequences are provided in Table S1.

Electrophoretic mobility shift assays

Double-stranded oligonucleotides were end-labeled with [γ^{32}P]ATP using T4-polynucleotide kinase. Nuclear or cytosolic protein extracts (2 µg; Supplementary material) were incubated for 15 min at room temperature in 20 µl binding buffer (30 mmol·L^{-1} HEPES, pH 7.5; 60 mmol·L^{-1} KCl; 0.5% glycerol; 0.1% Triton X100; 1 mmol·L^{-1} DTT), before the radiolabeled probe (0.5 ng) was added. Binding reactions were further incubated for 15 min with Rev-erbα (sc-135241) or Rev-erbβ antibodies (sc-47621, Santa-Cruz, Heidelberg, Germany) and resolved by 6% or 4% polyacrylamide gel electrophoresis in 0.25X Tris-Borate-EDTA buffer. Oligonucleotides are provided in the Supplementary material.

Fluorescence microscopy

Cells were fixed in 4% formaldehyde prior to staining with 4′,6-diamidino-2-phenylindole (DAPI) and AlexaFluor 488 labeled phalloidin and studied on a LSM-780 laser scanning microscope (Zeiss, Jena, Germany).

Electron microscopy

Scanning electron microscopy was performed on LEO-1530 and LEO-1450VP instruments (Zeiss, Oberkochen, Germany). Cells were grown on glass cover slips and fixed with 2.5% glutaraldehyde in 0.1 M cacodylate buffer. Samples were dehydrated in ascending ethanol concentrations, critical-point dried, and sputter coated with gold. Statistical image evaluation was conducted in 182 × 124 µm display windows (n = 5 to 13).

Statistical analysis

Statistical analysis was carried out using SigmaPlot (Systat, Erkrath, Germany). Data (mean ± SEM) were analyzed by *t* test, one-way ANOVA using Holm-Sidak *post hoc* analysis, or the corresponding non-parametric tests if criteria were violated. Correlation analysis was assessed with Pearson's product moment. *p* values below 0.05 were considered significant.

For further details regarding the materials and methods used, please refer to the Supplementary material and the CTAT table.

Results

BOXes occur under physiological conditions and increase in cholestasis

Concentrations of *Z*-BOX A and B in the systemic circulation have not been investigated yet. Therefore, we first determined serum/plasma concentrations of *Z*-BOX A and B in health, liver failure, and bilirubin conjugation failure (Fig. 1). The mean total serum concentration of *Z*-BOX A and B in healthy humans was 25.4 ± 3.4 nmol·L^{-1} (n = 10). We observed significantly higher concentrations of *Z*-BOX A and B (504.3 ± 30.3 nmol·L^{-1}, $p < 0.001$; n = 28) in patients with liver failure, which is associated with impaired hepatobiliary excretion (Fig. 1A, B). The mean total *Z*-BOX A and B concentrations in female (461.8 ± 54.7 nmol·L^{-1}; n = 11) were similar compared to those in male patients (531.8 ± 34.9 nmol·L^{-1}, $p < 0.26$, n = 17). Regarding the subgroup of alcoholic liver disease (418.5 ± 44.8 nmol·L^{-1}, n = 9) lower values compared to the other etiologies (544.9 ± 36.3 nmol·L^{-1}, $p = 0.049$; n = 19) were observed. Total concentrations of *Z*-BOX A and B in healthy Wistar rats (19.1 ± 4.6 nmol·L^{-1}; n = 12) and C57BL/6J mice (14.4 ± 0.8 nmol·L^{-1}; n = 5) did not differ from serum concentrations in healthy humans ($p > 0.85$). In contrast, the serum of Gunn rats with congenital hyperbilirubinemia exhibited significantly higher BOXes concentrations (136.9 ± 15.1 nmol·L^{-1}, $p < 0.001$; n = 14) compared to non-hyperbilirubinemic Wistar rats (Fig. 1C, D). In all samples, *Z*-BOX A and B concentrations strongly correlated with each other (r > 0.99; $p = 1{\cdot}10^{-55}$; Fig. 1F) and with the concentrations of unconjugated and total bilirubin (r > 0.86; $p = 4{\cdot}10^{-19}$; Fig. 1B, D; Fig. S2). Values of BOXes obtained in spiked corresponding serum and plasma samples did not differ from each other (concentrations in serum compared to those in plasma: *Z*-BOX A, 105.0 ± 3.1%, $p = 0.18$; *Z*-BOX B, 104.6 ± 2.3%, $p = 0.10$; n = 14 pairs; paired *t* test).

Yield of the regio-isomers in vitro

To better interpret blood concentrations of both regio-isomers in the light of PK/PD data we assessed their relative yield upon *in vitro* degradation of bilirubin with hydrogen peroxide, which led to formation of 1.5% *Z*-BOX A and 0.8% *Z*-BOX B, respectively.

The regio-isomers Z-BOX A and B have different pharmacokinetics

We then investigated whether the two regio-isomers *Z*-BOX A and B exhibit distinct pharmacokinetics. After *i.v.* bolus injection of equimolar *Z*-BOX A and B into rats, the peak serum concentrations of both compounds were reached at ~3.5 min (Fig. 2A, B). The serum disappearances exhibited clearly distinguishable distribution (α) and elimination (β) phases (inserts in Fig. 2A, B; Table. S2). Applying a two-compartment model, both compounds were dispersed in similar relative distribution volumes of ~1.0 L·kg^{-1} within the α phase (~15 min), tantamount to a uniform spread into the whole-body volume. Elimination parameters from first-order kinetics revealed a significantly lower serum half-live of *Z*-BOX A (31.0 ± 5.5 min) compared to *Z*-BOX B (55.4 ± 7.9 min, $p = 0.035$; n = 5; Fig. 2C). To foster interpretation of PK/PD, we determined water solubility (103.6 mg·L^{-1} and 76.4 mg·L^{-1}) and partition constants (log P_{OW} = 0.92 and 1.11) of *Z*-BOX A and B.

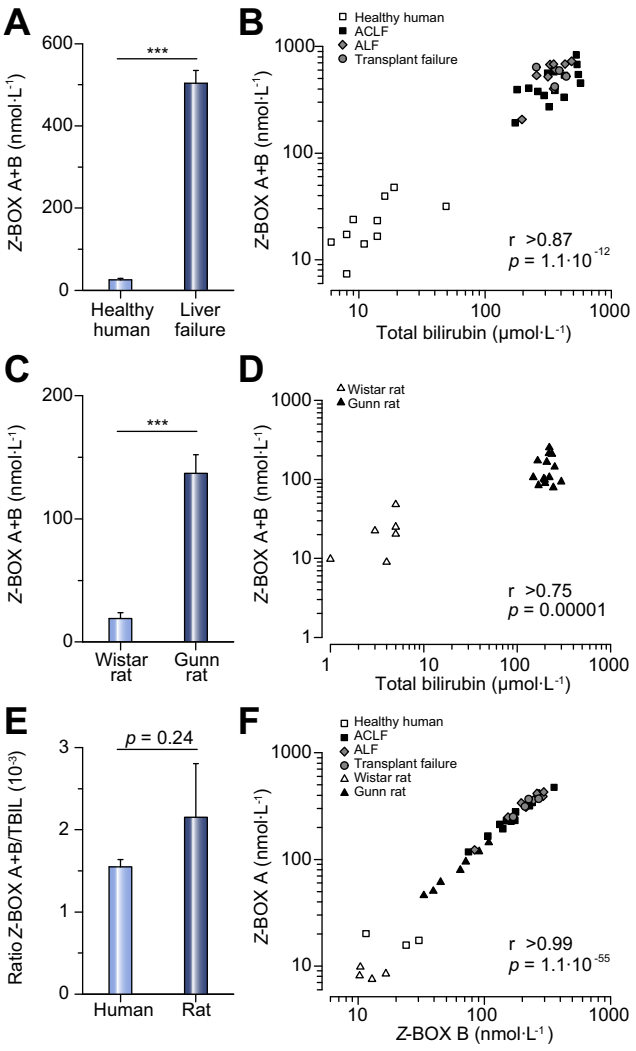

Fig. 1. *Z*-BOX A and *Z*-BOX B in health and cholestatic disease across species. (A) Mean concentrations of *Z*-BOX A + B in plasma of patients with liver failure (n = 28) compared to healthy controls (n = 10). ACLF, acute-on-chronic liver failure; ALF, acute liver failure. (B) *Z*-BOX A + B and bilirubin concentrations in the corresponding samples of human liver failure (filled symbols) compared to healthy controls (empty symbols). (C) Mean concentrations of *Z*-BOX A + B in serum/plasma samples of hyperbilirubinemic Gunn rats (animal model of Crigler-Najjar syndrome type I, n = 14) compared to non-hyperbilirubinemic Wistar rats (n = 12). (D) *Z*-BOX A + B and bilirubin concentrations in the corresponding samples of Gunn rats (filled symbols) compared to Wistar rats as control (empty symbols). (E) Cross-species comparison of the mean ratios between *Z*-BOX A + B and total bilirubin concentrations in human and rat samples. (F) Correlation between the *Z*-BOX A and B concentrations in all 38 human and 26 rat samples. Statistics: *t* test; ***$p < 0.001$; Pearson's *r* was calculated for the data in B, D, F.

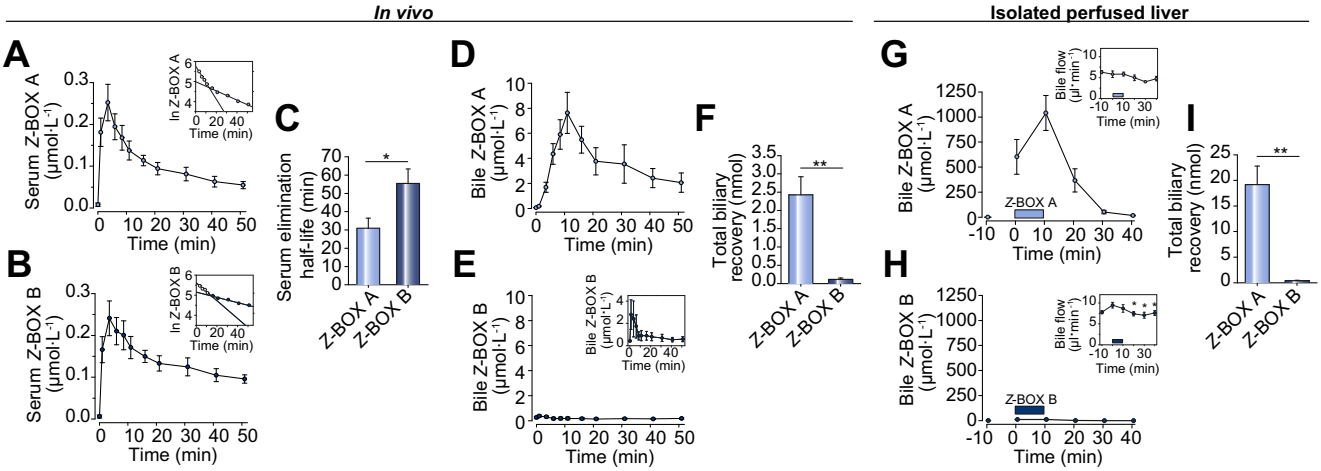

Fig. 2. Pharmacokinetics of *Z*-BOX A and *Z*-BOX B in rats. (A, B) Serum concentrations of *Z*-BOX A (A) and *Z*-BOX B (B) as a function of time after *i.v.* bolus injection of equimolar *Z*-BOX A and B (26.7 µg·(kg body weight)$^{-1}$) in Wistar rats at t = 0; insets illustrate distribution (empty symbols) and elimination (filled symbols) phases. (C) Mean serum elimination half-lives of *Z*-BOX A and B. (D, E) Biliary excretion profiles of *Z*-BOX A (D) and *Z*-BOX B (E) of the same experiments. Inset in E shows biliary *Z*-BOX B after administration of this isomer. (F) Mean absolute amounts of *Z*-BOX A and B excreted into bile. (G, H) Biliary excretion profiles of *Z*-BOX A (G) and *Z*-BOX B (H) upon individual perfusion of rat livers with 10 µmol·L^{-1} *Z*-BOX A (G) and *Z*-BOX B (H) for 10 min. Application of BOXes is indicated by the bars. Insets in G and H show bile flow as a function of time with the application of *Z*-BOX A and *Z*-BOX B, respectively. (I) Mean absolute amounts of *Z*-BOX A and B excreted into bile upon liver perfusion. Data points are mean ± SEM (A-F, n = 5; G-I, n = 3). Statistics: *t* test (C), Mann-Whitney *U* test (F, I), repeated measures ANOVA (insets in G, H); $^{*}p < 0.05$; $^{**}p < 0.01$.

BOXes are actively excreted into bile

Since *Z*-BOX A and B were cleared from the circulation after bolus injection, we asked whether biliary and urinary elimination occurred. We detected both compounds in the bile before and after *i.v.* bolus injection into rats. Notably, we found only trace amounts of these BOXes in corresponding urine samples of the same rats before (*Z*-BOX A + B, 8.4 ± 8.4 nmol·L^{-1}, n = 8) and 60 min after bolus injection (*Z*-BOX A + B, 14.7 ± 9.5 nmol·L^{-1}, $p > 0.64$; n = 8). Excretion of *Z*-BOX A and B into bile, however, was markedly different between the regio-isomers (Fig. 2D–F): *Z*-BOX A and B concentrations in bile before *i.v.* bolus (72.1 ± 8.4 nmol·L^{-1}; 320.2 ± 66.0 nmol·L^{-1}; n = 8) were significantly higher than the corresponding serum concentrations (4.8 ± 2.8 nmol·L^{-1}, $p < 0.001$; 12.0 ± 5.6 nmol·L^{-1}, $p < 0.001$; n = 8). *Z*-BOX A was enriched >30-fold and eliminated in bile with a mean peak concentration of 7.63 ± 1.64 µmol·L^{-1} (n = 5), measured 8.5 min after peak serum concentration (Fig. 2A, D). In contrast, *Z*-BOX B exhibited a different excretion profile and appeared at significantly lower peak concentrations in bile (371.7 ± 89.5 nmol·L^{-1}, measured 1.0 min after substance application; $p = 0.0022$, compared to *Z*-BOX A in bile; n = 5; Fig. 2D, E). To test whether the different excretion kinetics of *Z*-BOX A and B are due to competition between the regio-isomers, we solely injected *Z*-BOX B into rats in separate experiments (n = 3). In such experiments, bile concentrations of *Z*-BOX B were significantly increased (areas under the curves: 44.9 ± 18.9 µmol·L^{-1}·min *vs.* 8.72 ± 3.39 µmol·L^{-1}·min, $p = 0.047$; n = 3 and 5), albeit the excretion profiles were not different from those obtained after equimolar application of both regio-isomers (Fig. 2E, inset). Once the peak concentration of *Z*-BOX A was reached after *i.v.* bolus, the *Z*-BOX A concentrations in bile were consistently >30 times higher than in serum. Within ~50 min after injection of both regio-isomers, the overall amounts of non-metabolized compounds excreted into bile (Fig. 2F) were 42.9% (*Z*-BOX A) and 2.4% (*Z*-BOX B) of these BOXes in whole blood, reflecting 3.88% *Z*-BOX A and 0.18% *Z*-BOX B, respectively, of the administered molar amounts. In addition to the PK studies after single *i.v.* bolus, we determined the individual biliary excretion profiles upon 10-minute applications of *Z*-BOX A and B in isolated perfused rat livers (Fig. 2G–I). Perfusions with 10 µmol·L^{-1} BOXes resulted in the excretion of >100-fold enriched *Z*-BOX A (1.04 ± 0.17 mmol·L^{-1}, n = 3), whereas *Z*-BOX B (11.4 ± 2.3 µmol·L^{-1}, $p = 0.58$; n = 3) was not excreted actively into the bile.

Z-BOX A and B in human bile and gallstones

To confirm biliary excretion of *Z*-BOX A and B in humans without access to bile from healthy individuals, we determined *Z*-BOX A and B in bile samples obtained upon cholecystectomy. *Z*-BOX A (68.9–860 nmol·L^{-1}) and *Z*-BOX B (48.8–789 nmol·L^{-1}) were found in bile as well as in corresponding gallstones (Table S3, Fig. S3).

Z-BOX A and B do not alter portal hemodynamics

As *Z*-BOX A and B induce vasoconstriction of cerebral vessels[15] and as heme increases portal resistance (Schleser *et al.*, manuscript submitted) we hypothesized that *Z*-BOX A and B may alter portal hemodynamics. Isolated rat livers were perfused with *Z*-BOX A or B (Fig. 3A, B). Notably, the portal pressure did not change during the administrations or in the wash-out periods (*Z*-BOX A, $p = 0.38$; *Z*-BOX B, $p > 0.12$; referencing to baseline; n = 3).

Z-BOX A and B impair hepatocellular metabolism

We then asked whether *Z*-BOX A and B may affect hepatocellular integrity and metabolism. HepG2 cells responded to *Z*-BOX A and B with a dose-dependent increase of LDH release without significant differences between the regio-isomers (*Z*-BOX A,

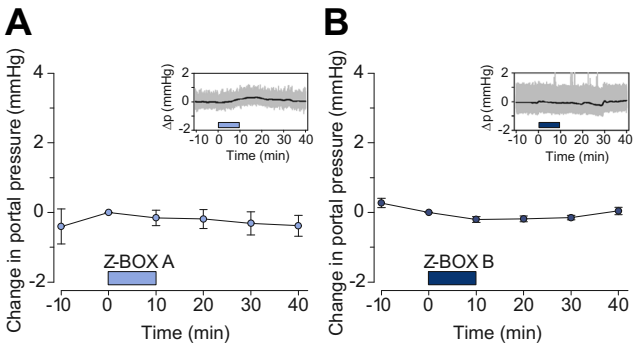

Fig. 3. Portal hemodynamics upon administration of *Z*-BOX A and *Z*-BOX B in rats. Isolated perfused livers were equilibrated for >10 min prior to treatment. (A, B) Changes in portal pressure upon perfusion with 10 μmol·L^{-1} *Z*-BOX A (A) and *Z*-BOX B (B). Application of BOXes is indicated by the bars. Insets in A, B display representative profiles of the raw (grey) and low-pass filtered (black) portal pressure. Data points are mean ± SEM (n = 3); Statistics: repeated measures ANOVA.

EC_{50} = 302 ± 125 μmol·L^{-1}; *Z*-BOX B, 179 ± 94 μmol·L^{-1}; n = 5). Of note, absolute cytotoxicity was marginal (Fig. 4A–C). The MTT assay revealed a dose-dependent impairment of metabolic rates with IC_{50} = 723 ± 283 μmol·L^{-1} (*Z*-BOX A; n = 3) and 509 ± 247 μmol·L^{-1} (*Z*-BOX B; n = 3), respectively (Fig. 4D–F).

Z-BOX A selectively affects hepatocellular cytoskeletal organization

As BOXes are significantly enriched in bile, the canalicular membranes of hepatocytes are subjected to much higher *Z*-BOX A and B concentrations compared to BOXes concentrations in blood. HepG2 cells reacted differently upon exposure to the regio-isomers *Z*-BOX A and B. While treatment with ≥125 μmol·L^{-1} *Z*-BOX A induced a morphological transformation from brick-like to spherically shaped cell morphology (Fig. 5) within few hours, the morphology of *Z*-BOX B-treated cells did not differ from control cells (Fig. 5A, B). Cells treated with *Z*-BOX A for 24 h were classified into three distinct groups: (I) Spherical cells with a strongly interfolded cell membrane and surface extensions distributed around the whole cell body associated with diminished cell-cell and cell surface contacts. (II) Cells of intermediate morphology with features of I and III. (III) Flatly attached cells with brick-like morphology (as the vehicle control) with brush border-like villi at the apical pole and numerous cell-cell contacts. In contrast, cells treated with *Z*-BOX B did not differ from the control (p >0.16; n = 543 and 744 individual cells/treatment; Fig. 5C). Notably, after *Z*-BOX A treatment for 48 h, the fraction of spherical cells did not change compared to 24-h incubation with *Z*-BOX A (p >0.14; n = 193 and 412 individual cells/treatment). However, after 48 h, three noticeable sub-types of the type I cells were distinguishable (Fig. S4): (a) cells with intact villi, (b) cells showing extensive blebbing of the cell membrane, and (c) cells without any visible cell surface extensions.

Morphological alterations are specific to hepatocytes

To confirm the *Z*-BOX A-specific effect in a second *in vitro* model, we investigated the bi-potent progenitor cell line HepaRG before and after terminal differentiation into its hepatocyte-like and biliary-like phenotypes. While undifferentiated HepaRG cells responded uniformly to *Z*-BOX A like HepG2, terminally differentiated HepaRG cells responded heterogeneously, depending on the particular phenotype. The morphology of the biliary-like phenotype, which served as an endogenous control, remained

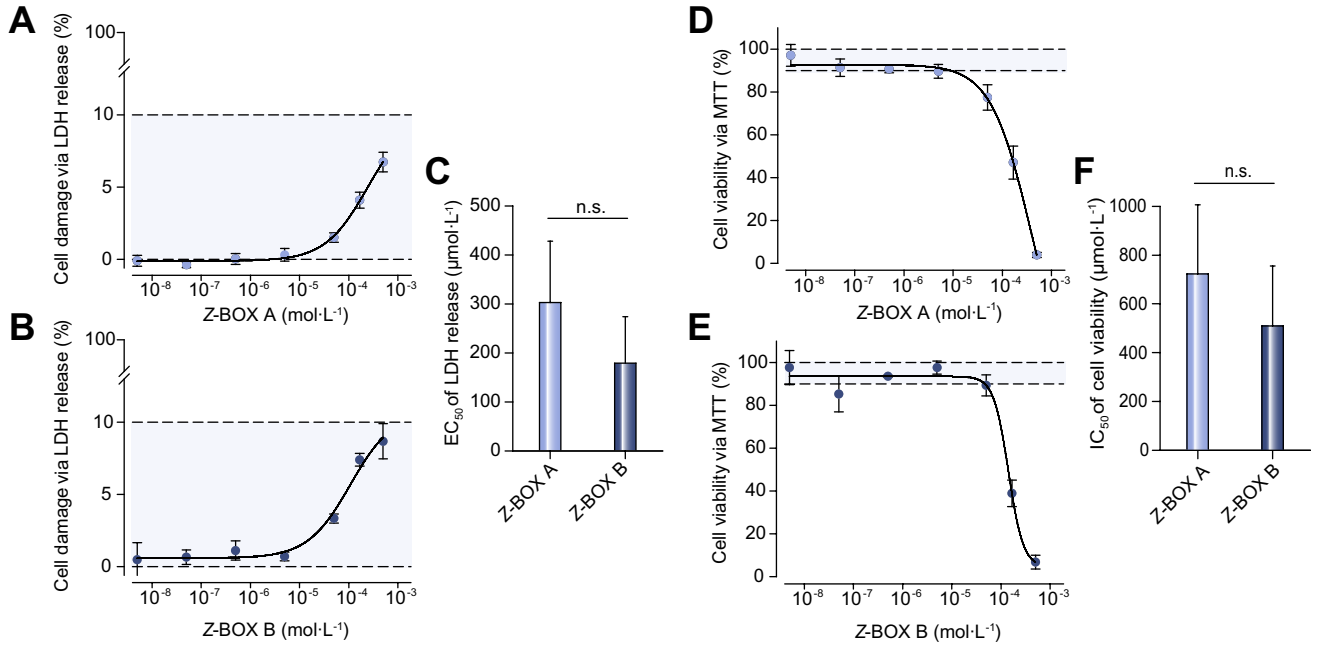

Fig. 4. Cytotoxicity and metabolic rate after incubation with *Z*-BOX A and B in HepG2 cells. (A, B) Dose-dependent LDH release as a surrogate of hepatocellular damage upon treatment with *Z*-BOX A (A) and *Z*-BOX B (B) for 96 h; superimposed sigmoid fits. (C) Mean half maximal effective concentrations of LDH release (n = 5) (D, E) Dose-dependent metabolic rate as measured by MTT assay upon treatment with *Z*-BOX A (C) and *Z*-BOX B (D) for 96 h; superimposed sigmoid fits. (F) Mean half maximal inhibitory concentrations of metabolic rate (n = 3). Light blue areas in A, B and D, E illustrate 10% change of the effect compared to control. Data are mean ± SEM. Statistics: *t* test.

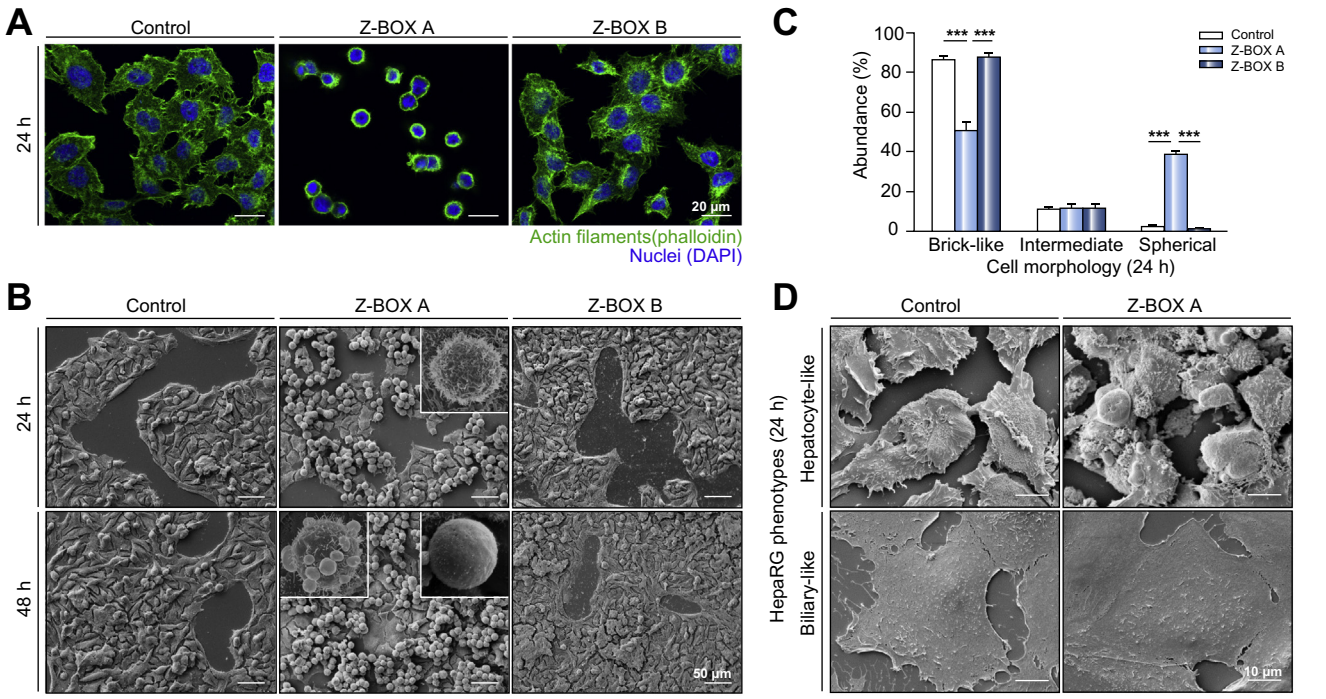

Fig. 5. The regio-isomer *Z*-BOX A alters specifically hepatocellular morphology. (A) Representative fluorescence micrographs of HepG2 cells after incubation with high-dose *Z*-BOX A, *Z*-BOX B, or control for 24 h. (B) Representative scanning electron micrographs of HepG2 cells after treatment with high-dose *Z*-BOX A, *Z*-BOX B, or control for 24 h. (C) Statistical evaluation of the different morphotypes (Brick-like, Intermediate, Spherical) after 24 h. (D) Representative scanning electron micrographs of terminally differentiated HepaRG cells after treatment with high-dose *Z*-BOX A or control for 24 h. The hepatocyte-like phenotype and the biliary-like phenotype (endogenous control) are growing in juxtaposition. Data are mean ± SEM (n = 502 to 744 cells/treatment); Statistics: one-way ANOVA; $^{***}p < 0.001$.

unaffected. The hepatocyte-like phenotype exhibited an altered morphology with a loss of cell-cell contacts and membrane blebbing (Fig. 5D).

BOXes interfere with the cytoplasmic glutathione redox potential

As the structures of *Z*-BOX A and B suggest reactivity towards thiol groups, we explored whether these BOXes affect the hepatocellular glutathione redox state. Using the genetically encoded fluorescent redox sensor Grx1-roGFP2,[23] we demonstrated that *Z*-BOX A and B significantly shift the glutathione redox potential to a more oxidized state (as measured via the formation of disulfide bonds in the fluorescent sensor) (Fig. 6A, Fig. S5). Applying LC and high-resolution MS, we further documented the formation of glutathione mono-adducts of both *Z*-BOX A and B *in vitro* (Fig. 6B, Fig. S6). The analyses revealed several successively eluting compounds with the same high-resolution mass. Tentative chemical structures and UV absorbance spectra of these adducts, which are similar to those of untransformed *Z*-BOX A and B,[19,20] are depicted in Figs. S6 and S7. Notably, *Z*-BOX A showed 10-fold higher reactivity towards glutathione than *Z*-BOX B (Fig. 6B). We also investigated whether *Z*-BOX A and B may increase lipid peroxidation in HepG2 cells (experimental details see Supplementary material). Direct incubations with these BOXes for 2 h did not result in significant changes of lipid peroxidation. After 24-h priming with *Z*-BOX A, the cells were (along with their changed morphology) less susceptible to oxidative stress, induced by *tert*-butylhydroperoxide (Fig. S8).

Z-BOX A and B modify gene expression by modulating the nuclear receptors Rev-erbα and Rev-erbβ

We hypothesized that, as demonstrated for heme, also the *Z*-BOX A or B regio-isomers may interact with members of the Rev-erb family of nuclear receptors. After exposure to either *Z*-BOX A or B, HIH showed a repression of the Rev-erbα and β target gene *PEPCK* ($p < 0.001$; n = 3; Fig. 6C).[25,26] Surprisingly, *Z*-BOX A and B differentially regulated mRNA expression of Rev-erbs itself: *Z*-BOX A repressed *Rev-erbα* ($p < 0.001$; n = 3) without affecting *Rev-erbβ* expression, while *Z*-BOX B had no impact on *Rev-erbα* or *β* gene expression. Furthermore, gene expression of several other targets of Rev-erbs (lipid metabolism genes fatty acid desaturase 2 [*FADS2*]; 3-hydroxy-3-methylglutaryl-CoA reductase [*HMGCR*]; the limiting step in bile acid synthesis cytochrome P450 isoenzyme 7A1 [*CYP7A1*]) was explored (Fig. 6C).[27] *FADS2* and *HMGCR* RNA expression were increased by *Z*-BOX B ($p < 0.001$; n = 3), while *Z*-BOX A did not affect their expression; however, both BOXes repressed CYP7A1 ($p < 0.001$; n = 3). We also performed electrophoretic mobility shift assays using revDR2 and its mutant variant abolishing Rev-erbs binding and cytosolic or nuclear extracts of HIH (Fig. 6D). Nuclear extracts of control cells weakly bound to the revDR2, while *Z*-BOX A nuclear extracts showed a strong binding, which was lost with revDR2 mutant. *Z*-BOX B nuclear extracts revealed two potential complexes of high and low size. Incubation with the revDR2 mutant identified the lower size complex as specific. Moreover, binding specificity was underlined by super-shift assays using antibodies against Rev-erbα or β and compared with the

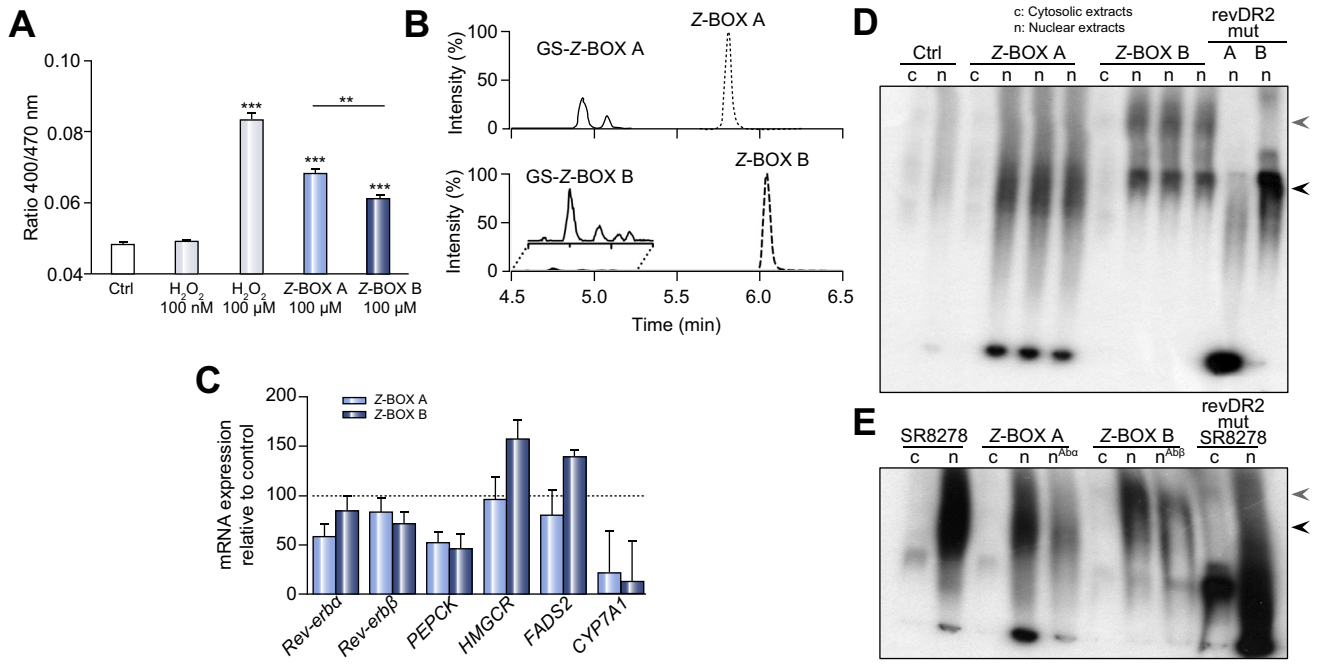

Fig. 6. *Z*-BOX A and B alter hepatocellular redox potential, differentially react with glutathione, and differentially modulate the activities of Rev-erbα and β. (A) Fluorescence ratio of the redox sensor Grx1-roGFP2 in HepG2 cells as a reporter of the intracellular glutathione redox potential; transfected HepG2 cells were incubated with each treatment at 37°C for 1 h prior to measuring the fluorescence ratio at room temperature. (B) Extracted ion current chromatograms with a mass tolerance of 2 ppm of *Z*-BOX A and B (m/z = 179.0815, dashed lines) and their stable mono-adducts with glutathione (m/z = 486.1653, solid lines) from LC-high-resolution-MS analysis after non-enzymatic incubation for 5 d. Multiple glutathione-BOXes adduct (GS-*Z*-BOX A/B) peaks indicate different diastereomers (magnification in inset, experimental details and further data see Supplementary material). (C) mRNA expression of *Rev-erbα*, *Rev-erbβ*, phosphoenolpyruvate carboxykinase (*PEPCK*), fatty acid desaturase 2 (*FADS2*), 3-hydroxy-3-methylglutaryl-CoA reductase (*HMGCR*), and *CYP7A1* in human immortalized hepatocytes (HIH) after stimulation with 15 µmol·L^{-1} *Z*-BOX A or B (n = 3 each) for 48 h (control cells set to 100). (D) Electrophoretic mobility shift assay of nuclear (n) or cytosolic (c) protein extracts (2 µg) of HIH upon treatment with or without 15 µmol·L^{-1} *Z*-BOX A or *Z*-BOX B using revDR2 and its mutant to repress binding of Rev-erbs. Arrows indicate binding of *Z*-BOX A (light blue) or *Z*-BOX B (dark blue). (E) Electrophoretic mobility super-shift assay using antibodies against Rev-erbα (Abα) or Rev-erbβ (Abβ) and the Rev-erbα modulator SR8278 and cytosolic (c) or nuclear (n) extracts of HIH treated with or without 15 µmol·L^{-1} of *Z*-BOX A or B. Arrows indicate reduced binding after pre-incubation with Rev-erbα (black) and Rev-erbβ (grey) antibodies. Data in A and C are mean ± SEM (A: n = 46 to 82; C; n = 3). Statistics: One-way ANOVA; $^{***}p$ <0.001.

Rev-erbα modulator SR8278 (Fig. 6E). Nuclear extracts of cells incubated with SR8278 showed a complex bound to revDR2, at the same molecular size as the *Z*-BOX A complex. *Z*-BOX A nuclear extract bound to revDR2, while pre-incubation of the nuclear extract with Rev-erbα antibody reduced binding – thus demonstrating that Rev-erbα was part of the complex and that its binding increased after *Z*-BOX A treatment. Similarly, *Z*-BOX B nuclear extract bound to the revDR2 oligos, while pre-incubation of the *Z*-BOX B extracts with a Rev-erbβ antibody abolished binding. Taken together, our results suggest that *Z*-BOX A acts as a modulator of Rev-erbα activity by increasing its binding to specific DNA response elements and repressing its own expression, while Z-BOX B increased the binding of Rev-erbβ and modulated gene expression of *FADS2* and *HMGCR*.

Discussion

The liver plays a key-role in heme catabolism, yielding equimolar amounts of biliverdin, ferrous iron, and carbon monoxide – each known to affect hepatic function or integrity.[28,29] However, there is a lack of data on formation, fate, and function of higher-order heme degradation products, in particular, of the regio-isomers *Z*-BOX A and *Z*-BOX B. Here, we characterize formation, kinetics, and impact of *Z*-BOX A and B on hepatic function and integrity. We demonstrate similar basal concentrations of *Z*-BOX A and B in healthy humans, rats, and mice. Substantially higher concentrations were found in patients with liver failure and in the Gunn rat model of congenital hyperbilirubinemia. Hepatocytes differently interacted with the regio-isomers *Z*-BOX A and B, leading to significantly different serum half-lives and biliary excretion profiles. While both acted as partial agonists of Rev-erbs and showed similar cytotoxicity, only *Z*-BOX A, which was strongly enriched in bile, triggered a characteristic remodeling of the hepatocellular cytoskeleton. Consistent with the altered cytoskeletal morphology and the effects on the central transcriptional regulators Rev-erbα and β that would suggest sustained impairment of excretory function, acute effects on bile production were observed *in vivo* (data not shown), but not in the isolated perfused liver preparation (Fig. 2G, H), in which the concentration of BOXes and bile salts remain constant. In contrast to single bolus injections, continued presence of endogenous *Z*-BOX A and B in patients and the substantial enrichment primarily of *Z*-BOX A may anticipate even stronger BOXes-triggered hepatocellular and extrahepatic effects under cholestatic conditions. As such, the molecular identification of Rev-erbα and β as targets of *Z*-BOX A and B is in line with their distinct pharmacokinetics. Rev-erbs are nuclear receptors coordinating lipid, glucose and bile acid synthesis, as well as phase I and II detoxification enzymes.[27] In addition, Rev-erbs are part of the circadian clock

system,[30] which is required to coordinate endo- and xenobiotic metabolism,[31] as evident in *Rev-erbα/β* double knock-out mice.[32,33] Intriguingly, Rev-erbs activation by *Z*-BOX A and B did not display the classical gene expression signature, leading to the hypothesis that *Z*-BOX A and B affected Rev-erbs differently. This might be due to the presence of endogenous ligands (heme and CO[34]) that are prevented from fully activating Rev-erbs by *Z*-BOX A and B through competition for the ligand binding domain access, or by modification of the oxidative stress, leading to changes in key cysteine residues of the ligand binding domain.[35] Repression of CYP7A1 as rate-limiting enzyme of bile acid synthesis by both BOXes may be considered a potentially protective mechanism against cholestasis with associated bile acid toxicity. Furthermore, the molecular reactivity of *Z*-BOX A and B towards thiol groups was shown with respect to glutathione, which constitutes the major hepatocellular redox system. As *Z*-BOX A and B altered the glutathione redox state different from direct oxidants, *e.g.* hydrogen peroxide at the same concentration, we hypothesize that *Z*-BOX A and B differently interfere with the glutathione system. *Z*-BOX A and B did neither increase lipid peroxidation after direct application nor led to a sensitization towards oxidative stress *in vitro*. We thus conclude that the formation of higher-order heme degradation products contributes to the detoxification of reactive oxygen species (ROS), despite their interaction with GSH.

Based on the cerebrovascular effects of BOXes,[14,15] we hypothesized that they might induce vasoconstriction in the portal circulation, which was however not the case. Although an in-depth interpretation of these divergent results in both vascular beds is beyond the scope of the present study, we propose that the nature of the effector cells, *i.e.* smooth muscle cells for the cerebrovascular effects and presumably hepatic stellate cells for the portal hemodynamics, might explain this discrepancy. Although BOXes might affect terminal portal venules, available evidence would point towards a primary action of heme[36] and first-order degradation products, in particular CO,[37] act primarily on hepatic stellate cells with a distinctly different contractile apparatus compared to smooth muscle cells.

Hepatocytes reacted differently towards the regio-isomers *Z*-BOX A and B. The specificity for regio-isomers is distinctly demonstrated by the differential binding to Rev-erbα and β, respectively. Furthermore, the pharmacokinetic characteristics of *Z*-BOX A and B showed significant differences in serum disappearance rates and biliary excretion.

The mechanism of bilirubin degradation through ROS-mediated conversions has not been elucidated yet. Based on the different chemical yields of the regio-isomers after *in vitro* degradation of bilirubin, we assume that *Z*-BOX A is also formed in a twofold excess *in vivo*. The approximately twofold shorter serum half-live of *Z*-BOX A compared to *Z*-BOX B is expected to compensate these unequal production rates leading to similar equilibrium concentrations of both regio-isomers in the bloodstream as observed in the present study (Fig. 1). We demonstrated in rats that elimination into the bile substantially contributes to the serum clearance, in particular of *Z*-BOX A. Although the baseline concentrations of *Z*-BOX B in bile were approximately four times higher than those of *Z*-BOX A, primarily *Z*-BOX A was excreted and strongly enriched in the bile after *i.v.* bolus administration. The fact that *Z*-BOX B concentrations were significantly higher if solely *Z*-BOX B was administered strongly indicates a competition between both regio-isomers. Although the mechanistic background for the preference of *Z*-BOX A remains to be elucidated, we conclude that the presence of *Z*-BOX A suppresses the excretion of its isomer, *Z*-BOX B. The serum disappearance of *Z*-BOX B without marked excretion of the unchanged molecule into bile strongly suggests further metabolic conversions prior to its elimination. The immediate and selective enrichment of *Z*-BOX A in bile illustrates the availability of suitable transport mechanisms to lower serum concentrations. It further supports the notion that higher concentrations, as required for the rearrangement of the canalicular cell pole, can be achieved locally *in vivo*. Human bile samples from patients subjected to cholecystectomy exhibited moderately higher concentrations of *Z*-BOX A compared to *Z*-BOX B, which is in contrast to the baseline concentrations of these compounds in the bile of rats. Beyond an altered composition of the pathologic bile samples, this discrepancy may be due to potential formation of these BOXes from heme-derived tetrapyrroles, intermediate bilirubin oxidation products, or intestinal microbiota.

To support hepatocellular excretion into bile, microvilli provide a surface enhancement on the canalicular pole to facilitate transporter insertion and substance delivery.[38] Upon *Z*-BOX A treatment, HepG2 cells reacted with the reorganization of their actin cytoskeleton, leading to formation of spherical cell bodies and loss of polarity. It is noteworthy that these effects were observed in the HepG2 cell line at substantially higher concentrations than those measured in patient plasma. However, the substantial (~100-fold) enrichment of *Z*-BOX A across the hepatocellular route of excretion as well as the very long exposure intervals under conditions of cholestasis support the potential biological significance of alterations in brush border morphology. This effect was confirmed in a second cell line, *i.e.* terminally differentiated HepaRG cells, where the biliary-like phenotype represented an endogenous control.[39] The diverging reactivity of these two phenotypes towards *Z*-BOX A treatment is consistent with the presence of specific up-take systems for *Z*-BOX A that seem to be restricted to the hepatocyte-like phenotype. Hepatocellular stress induced by BOXes may impair bile secretory function. Interestingly, such cholestatic effects of BOXes may resemble cholestatic liver and bile duct injury induced by precursors of heme, in particular, protoporpyrins accumulating due to hereditary absence or chemical inhibition of ferrochelatase activity in humans with or mouse models of erythropoietic protoporphyria.[40]

In summary, we demonstrate that *Z*-BOX A and B are bioactive endogenous degradation products of heme that differently interact with the liver. Consequently, our data introduce the concept that cytotoxic effects so far solely attributed to bilirubin might, at least in part, be mediated by higher-order degradation products of heme.

Financial support

This study was supported by the German Research Foundation, within the framework of the Research Unit FOR 1738 (to MB, SMC, SHH, GP, and MW), and the Austrian Science Foundation, grant F3517-B20 (to MT).

Conflict of interest

The authors who have taken part in this study declared that they do not have anything to disclose regarding funding or conflict of interest with respect to this manuscript.

Please refer to the accompanying ICMJE disclosure forms for further details.

Authors' contributions

Designed research: RAS, TC, SHH, GP, MT, MB. Performed experiments: RAS, TC, FAS, NKO, SN. Sample recruitment: RAS, MW, CS, FC, SMC. Wrote the manuscript: RAS, TC, SN, SHH, GP, MT, MB.

Acknowledgements

We thank Maurice Klopfleisch for providing crude synthetic BOXes, Michael Kiehntopf for bilirubin measurements, Falk Rauchfuß and Utz Settmacher for providing bile and gallstone samples, Danny Himsel for technical support during PK/PD studies, and Sebastian Weis for critically reviewing the manuscript. We acknowledge Alexander Mosig for the cooperation during investigator-initiated experiments with HepaRG cells to study *in vitro* models of liver dysfunction.

Supplementary data

Supplementary data associated with this article can be found, in the online version, at http://dx.doi.org/10.1016/j.jhep.2017.03.037.

References

Author names in bold designate shared co-first authorship

[1] Girvan HM, Munro AW. Heme sensor proteins. J Biol Chem 2013;288:13194–13203.
[2] Soares MP, Bozza MT. Red alert: labile heme is an alarmin. Curr Opin Immunol 2016;38:94–100.
[3] Larsen R, Gozzelino R, Jeney V, Tokaji L, Bozza FA, Japiassu AM, et al. A central role for free heme in the pathogenesis of severe sepsis. Sci Transl Med 2010;2:1–12.
[4] Schaer DJ, Vinchi F, Ingoglia G, Tolosano E, Buehler PW. Haptoglobin, hemopexin, and related defense pathways-basic science, clinical perspectives, and drug development. Front Physiol 2014;5:415.
[5] **Seixas E**, **Gozzelino R**, Chora A, Ferreira A, Silva G, Larsen R, et al. Heme oxygenase-1 affords protection against noncerebral forms of severe malaria. Proc Natl Acad Sci U S A 2009;106:15837–15842.
[6] Bauer I, Wanner GA, Rensing H, Alte C, Miescher EA, Wolf B, et al. Expression pattern of heme oxygenase isoenzymes 1 and 2 in normal and stress-exposed rat liver. Hepatology 1998;27:829–838.
[7] Dey S, Bindu S, Goyal M, Pal C, Alam A, Iqbal MS, et al. Impact of intravascular hemolysis in malaria on liver dysfunction: involvement of hepatic free heme overload, NF-κB activation, and neutrophil infiltration. J Biol Chem 2012;287:26630–26646.
[8] Di Pascoli M, Zampieri F, Quarta S, Sacerdoti D, Merkel C, Gatta A, et al. Heme oxygenase regulates renal arterial resistance and sodium excretion in cirrhotic rats. J Hepatol 2011;54:258–264.
[9] Gozzelino R, Jeney V, Soares MP. Mechanisms of cell protection by heme oxygenase-1. Annu Rev Pharmacol Toxicol 2010;50:323–354.
[10] Baranano DE, Rao M, Ferris CD, Snyder SH. Biliverdin reductase: a major physiologic cytoprotectant. Proc Natl Acad Sci U S A 2002;99:16093–16098.
[11] Horsfall LJ, Hardy R, Wong A, Kuh D, Swallow DM. Genetic variation underlying common hereditary hyperbilirubinaemia (Gilbert's syndrome) and respiratory health in the 1946 British birth cohort. J Hepatol 2014;61:1344–1351.
[12] Erlinger S, Arias IM, Dhumeaux D. Inherited disorders of bilirubin transport and conjugation: new insights into molecular mechanisms and consequences. Gastroenterology 2014;146:1625–1638.
[13] Watchko JF, Tiribelli C. Bilirubin-induced neurologic damage - mechanisms and management approaches. N Engl J Med 2013;369:2021–2030.
[14] Clark JF, Sharp FR. Bilirubin oxidation products (BOXes) and their role in cerebral vasospasm after subarachnoid hemorrhage. J Cereb Blood Flow Metab 2006;26:1223–1233.
[15] Joerk A, Seidel RA, Walter SG, Wiegand A, Kahnes M, Klopfleisch M, et al. Impact of heme and heme degradation products on vascular diameter in mouse visual cortex. J Am Heart Assoc 2014;3.
[16] Hou S, Xu R, Clark JF, Wurster WL, Heinemann SH, Hoshi T. Bilirubin oxidation end products directly alter K^+ channels important in the regulation of vascular tone. J Cereb Blood Flow Metab 2011;31:102–112.
[17] Kranc KR, Pyne GJ, Tao L, Claridge TD, Harris DA, Cadoux-Hudson TA, et al. Oxidative degradation of bilirubin produces vasoactive compounds. Eur J Biochem 2000;267:7094–7101.
[18] Lakovic K, Ai J, D'Abbondanza J, Tariq A, Sabri M, Alarfaj AK, et al. Bilirubin and its oxidation products damage brain white matter. J Cereb Blood Flow Metab 2014;34:1837–1847.
[19] Klopfleisch M, Seidel RA, Gorls H, Richter H, Beckert R, Imhof W, et al. Total synthesis and detection of the bilirubin oxidation product (Z)-2-(3-ethenyl-4-methyl-5-oxo-1,5-dihydro-2H-pyrrol-2-ylidene)ethanamide (Z-BOX A). Org Lett 2013;15:4608–4611.
[20] **Seidel RA**, **Schowtka B**, **Klopfleisch M**, Kuhl T, Weiland A, Koch A, et al. Total synthesis and characterization of the bilirubin oxidation product (Z)-2-(4-ethenyl-3-methyl-5-oxo-1,5-dihydro-2H-pyrrol-2-ylidene)ethanamide (Z-BOX B). Tet Lett 2014;55:6526–6529.
[21] Seidel RA, Kahnes M, Bauer M, Pohnert G. Simultaneous determination of the bilirubin oxidation end products Z-BOX A and Z-BOX B in human serum using liquid chromatography coupled to tandem mass spectrometry. J Chromatogr B 2015;974:83–89.
[22] **Cuperus FJC**, **Schreuder AB**, van Imhoff DE, Vitek L, Vanikova J, Konickova R, et al. Beyond plasma bilirubin: The effects of phototherapy and albumin on brain bilirubin levels in Gunn rats. J Hepatol 2013;58:134–140.
[23] Gutscher M, Pauleau AL, Marty L, Brach T, Wabnitz GH, Samstag Y, et al. Real-time imaging of the intracellular glutathione redox potential. Nat Methods 2008;5:553–559.
[24] Schippers IJ, Moshage H, Roelofsen H, Muller M, Heymans HSA, Ruiters M, et al. Immortalized human hepatocytes as a tool for the study of hepatocytic (de-)differentiation. Cell Biol Toxicol 1997;13:375–386.
[25] Raghuram S, Stayrook KR, Huang P, Rogers PM, Nosie AK, McClure DB, et al. Identification of heme as the ligand for the orphan nuclear receptors REV-ERBα and REV-ERBα. Nat Struct Mol Biol 2007;14:1207–1213.
[26] Yin L, Wu N, Curtin JC, Qatanani M, Szwergold NR, Reid RA, et al. Rev-erbα, a heme sensor that coordinates metabolic and circadian pathways. Science 2007;318:1786–1789.
[27] Le Martelot G, Claudel T, Gatfield D, Schaad O, Kornmann B, Lo Sasso G, et al. REV-ERBα participates in circadian SREBP signaling and bile acid homeostasis. PLoS Biol 2009;7 e1000181.
[28] Tenhunen R, Marver HS, Schmid R. The enzymatic conversion of heme to bilirubin by microsomal heme oxygenase. Proc Natl Acad Sci U S A 1968;61:748–755.
[29] Bauer M, Kiehntopf M. Shades of yellow: monitoring nutritional needs and hepatobiliary function in the critically ill. Hepatology 2014;60:26–29.
[30] Preitner N, Damiola F, Luis Lopez M, Zakany J, Duboule D, Albrecht U, et al. The orphan nuclear receptor REV-ERBα controls circadian transcription within the positive limb of the mammalian circadian oscillator. Cell 2002;110:251–260.
[31] Claudel T, Cretenet G, Saumet A, Gachon F. Crosstalk between xenobiotics metabolism and circadian clock. FEBS Lett 2007;581:3626–3633.
[32] Bugge A, Feng D, Everett LJ, Briggs ER, Mullican SE, Wang F, et al. Rev-erbα and Rev-erbβ coordinately protect the circadian clock and normal metabolic function. Genes Dev 2012;26:657–667.
[33] Cho H, Zhao X, Hatori M, Yu RT, Barish GD, Lam MT, et al. Regulation of circadian behaviour and metabolism by REV-ERB-α and REV-ERB-α. Nature 2012;485:123–127.
[34] Pardee KI, Xu X, Reinking J, Schuetz A, Dong A, Liu S, et al. The structural basis of gas-responsive transcription by the human nuclear hormone receptor rev-erbα. PLoS Biol 2009;7 e43.
[35] Gupta N, Ragsdale SW. Thiol-disulfide redox dependence of heme binding and heme ligand switching in nuclear hormone receptor rev-erbbeta. J Biol Chem 2011;286:4392–4403.

[36] Schleser FA, Seidel RA, Press AT, Heinemann SH, Clemens M, Bauer M. Contribution of free heme to impaired microcirculation and hepatic injury in sepsis. Shock 2015;43:25.
[37] Suematsu M, Goda N, Sano T, Kashiwagi S, Egawa T, Shinoda Y, et al. Carbon monoxide: an endogenous modulator of sinusoidal tone in the perfused rat liver. J Clin Invest 1995;96:2431–2437.
[38] **Recknagel P**, **Gonnert FA**, Westermann M, Lambeck S, Lupp A, Rudiger A, et al. Liver dysfunction and phosphatidylinositol-3-kinase signalling in early sepsis: experimental studies in rodent models of peritonitis. PLoS Med 2012;9 e1001338.
[39] Dianat N, Dubois-Pot-Schneider H, Steichen C, Desterke C, Leclerc P, Raveux A, et al. Generation of functional cholangiocyte-like cells from human pluripotent stem cells and HepaRG cells. Hepatology 2014;60:700–714.
[40] Meerman L, Koopen NR, Bloks V, van Goor H, Havinga R, Wolthers BG, et al. Biliary fibrosis associated with altered bile composition in a mouse model of erythropoietic protoporphyria. Gastroenterology 1999;117:696–705.